PNAS
www.pnas.org

Supplementary Information for

SRS-FISH: A High-Throughput Platform Linking Microbiome Metabolism to Identity at the Single Cell Level

Xiaowei Ge, Fátima C. Pereira, Matthias Mitteregger, David Berry, Meng Zhang, Bela Hausmann, Jing Zhang, Arno Schintlmeister, Michael Wagner and Ji-Xin Cheng

Michael Wagner and Ji-Xin Cheng
E-mail: michael.wagner@univie.ac.at, jxcheng@bu.edu

This PDF file includes:

Supplementary Methods

SRS-FISH platform sensitivity and spatial resolution. To evaluate the limit of detection for C-D and C-H bonds by our femtosecond SRS setup, measurements of DMSO/H_2O mixtures in the concentration range from 0.004 to 4 M were conducted, each for isotopically unlabeled DMSO (purity ≥99.9%, D8418-500ML, Sigma-Aldrich) and fully deuterated DMSO (DMSO-d6, 99.96 atom % D, 156914-1G, Sigma-Aldrich). Ultrapure water was utilized as blank. Statistical analysis of the obtained datasets revealed a significant enhancement of the signal intensities already for the 4 mM samples relative to the blank (one-sided Z-test, $p = 3.59\times10^{-4}$ for DMSO and $p = 1.31\times10^{-4}$ for d6-DMSO). Taking into account the SRS excitation volume of 0.18 μm^3 (estimated from the lateral and axial beam profiles, Fig. S1), the minimum amount of C-H and C-D bonds detectable by femtosecond SRS imaging amounts to 2.6×10^6 per pixel.

To determine the SRS lateral resolution, 200 nm polymethyl methacrylate beads (MMA200, Degradex phosphorex, USA) were used. By deconvoluting the SRS image with simulated 200 nm size beads, we obtained the point spread function (PSF) of SRS (1), which was the product of pump and Stokes beam and had a FWHM around 242.3 nm (Fig. S1). With 210 nm yellow green fluorescence beads (17151-10, Polysciences, USA), the lateral and axial resolution of non-degenerate (ND)-TPEF, pump beam TPEF, and Stokes beam TPEF were measured in the liquid or dry conditions. The ND-TPEF was also the product of pump and Stokes beam, thus it is similar to SRS PSF measurement. Then ND-TPEF images were obtained by subtracting fluorescence images with pump and Stokes both on by pump only TPEF images and Stokes only TPEF images. Due to the broad two-photon absorption, we could detect fluorescence using different laser beams, under both liquid and dry imaging conditions, although signal from the 1045 nm TPEF beam in dry conditions was too weak to see the fluorescence beads. The resolution was calculated following the steps of SRS resolution calculation. In the liquid environment, the lateral resolutions of pump only TPEF, Stokes only TPEF, and ND-TPEF by pump and Stokes were 300∼400 nm while all of them degraded 1.5∼2 times to 500 nm∼600 nm when imaging in the dry conditions. The axial resolutions degraded by 3 times from ∼1.8 μm in the liquid environment to ∼6 μm in the dry conditions (Fig. S1). This measurement further demonstrated the degraded sensitivity of SRS when imaging in the dry conditions. Meanwhile, TPEF degradation in the dry conditions did not impede the precision of generating FISH masks (Fig. S1, Fig. S6A, S7) (2), which also has a lower requirement of signal level.

Growth and labeling of microbial pure cultures. *Escherichia coli* K12 (DSM 498) was grown aerobically at 37°C in Luria-Bertani liquid medium (LB; DSMZ medium 381) or M9 minimal medium containing per L of medium: 7.5 g $Na_2HPO_4.2H_2O$, 3 g KH_2PO_4, 0.5 g NaCl, 0.5 g NH_4Cl, 1 mM $MgSO_4$, 0.3 mM $CaCl_2$, 1 mg thiamine hydrochloride (Sigma-Aldrich), 1 mg biotin (Sigma-Aldrich), trace elements, 0.4% (w/v) D-Glucose (Carl Roth GmbH). For D labeling of *E. coli* cultures, 50 μl of a stationary-phase culture were used to inoculate 5mL of LB or M9 medium containing different percentages (vol/vol) of D_2O (99.9 at% D; Sigma Aldrich). Cells were grown until the late exponential phase (3 h in LB medium or 8-10 h in M9 medium), harvested by centrifugation and fixed in 4% formaldehyde in phosphate-buffered saline (PBS) for 2 h at 4°C. Cells were subsequently washed once with PBS and stored at 4°C until further use. *Bacteroides thetaiotaomicron* (DSM 2079) cells were grown anaerobically (85% N_2, 10% CO_2, 5% H_2) in BHI broth (DSMZ medium 215c) or in *Bacteroides* minimal medium (3) containing different percentages (vol/vol) of D_2O (99.9 at% D; Sigma Aldrich). After 6 hours of growth at 37°C, cells were harvested by centrifugation, resuspended in PBS, and fixed by adding formaldehyde in PBS as described above. All cells were stored in a PBS solution at 4°C until further use. *Clostridium scindens* (ATCC35704, kindly provided by Prof. Bärbel Stecher, Max-vonPettenkofer Institute, LMU Munich, Germany) and *Blautia producta* (isolate Y6.3- GenBank accession number OM489277) cells were grown anaerobically (85% N_2, 10% CO_2, 5% H_2) in BHI broth (DSMZ medium 215c) or in *Bacteroides* minimal medium (3) supplemented with 5 g per litre of casaminoacids (MP Biomedicals™) (BMMs) containing different concentrations (vol/vol) of D_2O (99.9% atom % (at%) D; Sigma Aldrich). Supplementation with casaminoacids was necessary as for *C. scindens* and *B. producta* to grow on BMM, as these organisms were either predicted or shown to be auxotrophs for some amino acids (4, 5). After approximately 8 or 12 hours of growth at 37°C in either BHI or BMMs, *C. scindens* cells were harvested by centrifugation, resuspended in PBS, and fixed by adding formaldehyde in PBS as described above. *B. producta* cells were harvested following the same procedure, but after 5 or 8 hours of growth at 37°C in either BHI or BMMs.

Gut microbiome incubations. Human fecal samples were collected from three healthy adult individuals (one male and two females between the ages of 25 to 38) who had not received antibiotics in the prior 3 months. Study participants provided informed consent and self-sampled using an adhesive paper-based feces catcher (FecesCatcher, Tag Hemi, Zeijen, NL) and a sterile polypropylene tube with the attached sampling spoon (Sarstedt, Nümbrecht, DE). The study protocol was approved by the University of Vienna Ethics Committee (reference No.00161). All meta(data) is 100% anonymized and compliant with the University's regulations. Samples were transferred into a n anaerobic tent (Coy Laboratory Products, USA) within 30 min after sampling. Samples were suspended in M9 medium (prepared with H_2O and without glucose) to achieve a concentration of 0.1 g.ml-1, and further diluted 20 times in this medium. The homogenate was left to settle for 10 minutes, and the supernatant was then distributed into glass vials. An equal volume of M9 (without glucose) prepared with either D_2O (99.9 at% D; Sigma Aldrich) or H_2O (for the negative control) was added to each tube, and each vial was finally supplemented with different concentrations of mucosal sugar monosaccharides (N-acetylneuraminic acid: 2 $mg.ml^{-1}$; N-acetylglucosamine: 5 $mg.ml^{-1}$; fucose: 2.5 $mg.ml^{-1}$; galactose: 5 $mg.ml^{-1}$; N-acetylgalactosamine: 2.5 $mg.ml^{-1}$), D-glucose (5 $mg.ml^{-1}$) or nothing (no-amendment control) (all amendment chemicals were from Sigma–Aldrich, except D(+)-galactose which was purchased from Carl Roth GmbH). These concentrations were selected based on reported concentrations of the different monosaccharides

in purified hog gastric mucin and mucin gels, as described in (6). Once all incubations were set, an aliquot sample from the negative control was immediately collected, pelleted and stored at -20°C until further use (T0 sample). After incubation for 6 h at 37°C under anaerobic conditions (5% H2, 10% CO2, 85% N2), two sample aliquots from each incubation were collected by centrifugation. One aliquot washed with 1× PBS to remove D_2O and then fixed in 4% formaldehyde for 2 h at 4°C. Samples were finally washed two times with 1 ml of PBS and stored in PBS at 4°C until further use. The second aliquot was stored at -20°C until further processing.

Confocal fluorescence microscopy. Samples were spotted onto microscope slides (Paul Marienfeld EN) with Poly-L-lysine coating and visualized using an Olympus scanning confocal microscope (FV3000) with a 60x oil objective (PLAPON60XO, 1.42 NA, 0.15 mm WD, Olympus) and two high-sensitivity photomultiplier tubes (PMTs). Cy3 double-labeled probe Bac303 was excited by a 514 nm solid state diode laser and its emission was collected between 530 nm and 630 nm. Cy5 double-labeled probe Erec482 was excited by a 640 nm solid state diode laser and its emission was collected between 650 nm and 750 nm. Transmission images were also collected for validating the focus and the distribution of the whole gut microbiome sample. The ideal spatial resolution limit is around 221 nm∼275 nm. The scanning step size of the confocal image was set to 103.58 nm, which was smaller than half of the diffraction limit of both beams and ensured sampling spatial frequency higher than the Nyquist frequency for both excitation wavelengths. Each acquired field of view is $212^2 \mu m^2$.

Spontaneous Raman microspectroscopy. Fixed cells were spotted on aluminum-coated slides (Al136; EMF Corporation). Excess of salt was removed by dipping the slide twice into ice-cold Milli-Q water. Individual cells were observed under a 100×/0.75 NA microscope air objective Single microbial cell spectra were acquired using a LabRAM HR800 confocal Raman microscope (Horiba Jobin-Yvon) equipped with a 532 nm neodymium-yttrium aluminum garnet (Nd:YAG) laser and 300 grooves/mm diffraction grating. Spectra were acquired in the range of 400–3200 cm^{-1} for 30 s with 2.18 mW laser power. Spectra were then aligned according to the phenylalanine peak regionand, a background correction using the sensitive nonlinear iterative peak-clipping algorithm was applied as described before (7). Spectra were then normalized by dividing the spectral intensity at each wavelength by the total spectral intensity. For quantification of the degree of D incorporation into the cells, %CD was calculated using the integration of the intensity of bands assigned to C–D (2040–2300 cm^{-1}) and C–H (2800–3100 cm^{-1}) (7). For Raman-FISH analyses, cells displaying signals originating from hybridized oligonucleotide probes were identified using epifluorescence imaging on the Raman confocal microscope equipped with a 100-W Xenon lamp, a standard Cy5 filter block and an F-View camera (Soft Imaging Systems). Raman spectra of targeted cells were obtained by switching image acquisition to the inbuilt Raman CCD detector.

Amplification and sequencing of the 16S rRNA genes. Pellets of microbiome incubation samples were resuspended in 1mL of InhibitEX Buffer (Qiagen) and subjected to bead beating for 40 seconds at 6 m/s in Lysis matrix E (MPBiomedicals) tubes. DNA extraction was performed with the QiaAMP Fast DNA Stool Kit (Qiagen) according to the manufacturers protocol. Amplification of bacterial 16S rRNA genes from DNA extracts was performed with a two-step barcoding approach (UDB-H12) (8). V1-V3 amplicons were made using the 27F (5'-AGAGTTTGATCCTGGCTCAG-3') (9) and 534R (5'-ATTACCGCGGCTGCTGG-3') (10) primers, including a 5'-head sequence for 2-step PCR barcoding. PCRs, barcoding, library preparation and Illumina MiSeq sequencing were performed by the Joint Microbiome Facility (Vienna, Austria) under project number JMF-2110-18. First-step PCRs were performed in triplicate (12.5 μL vol per reaction) with the following conditions: 1× DreamTaq Buffer (Thermo Fisher), 2 mM $MgCl_2$ (Thermo Fisher), 0.2 mM dNTP mix (Thermo Fisher), 0.2 μM of forward and reverse primer each, 0.08 mg mL^{-1} Bovine Serum Albumin (Thermo Fisher), 0.02 U Dream Taq Polymerase (Thermo Fisher), and 0.5 μL of DNA template. Conditions for thermal cycling were: 95°C for 3 min, followed by 30 cycles of 30 s at 95°C, 30 s at 52°C and 50 s at 72°C, and finally 10 min at 72°C. Triplicates were combined for barcoding (with 8 PCR cycles). Barcoded samples were purified and normalized over a SequalPrep Normalization Plate Kit (Invitrogen) using a Biomek NXP Span-8 pipetting robot (Beckman Coulter), and pooled and concentrated on PCR purification columns (Analytik Jena). Indexed sequencing libraries were prepared with the Illumina TruSeq Nano Kit as described previously (11), and sequenced in paired-end mode (2× 300 bp; v3 chemistry) on an Illumina MiSeq following the manufacturer's instructions. The workflow systematically included four negative controls (PCR blanks, i.e., PCR-grade water as template) for each 90 samples sequenced. The 16S rRNA gene sequences were deposited in the NCBI Sequence Read Archive (SRA) as BioProject Accession PRJNA802995.

Analysis of 16S rRNA gene amplicon sequences. Amplicon pools were extracted from the raw sequencing data using the FASTQ workflow in BaseSpace (Illumina) with default parameters (8). Input data was filtered for PhiX contamination with BBDuk (BBTools, Bushnell B, sourceforge.net/projects/bbmap). Demultiplexing was performed with the python package demultiplex (Laros JFJ, github.com/jfjlaros/demultiplex) allowing one mismatch for barcodes and two mismatches for linkers and primers. DADA2 R package version 1.16.0 (https://www.r-project.org/, R 4.0.2) (12) was used for demultiplexing amplicon sequencing variants (ASVs) using a previously described standard protocol (13). FASTQ reads were trimmed at 150 nt with allowed expected errors of 2. Taxonomy was assigned to 16S rRNA gene sequences based on SILVA taxonomy (release 138) using the DADA2 classifier (12). Sequencing of an extraction control yielded only 0 reads. Relative abundances of each taxa in a sample were calculated after correcting for the different number of copies of the 16S rRNA, according to rrnDB (version 5.7). Amplicon sequence libraries were rarefied to 2130 reads per sample and analyzed using the vegan (v2.5-.6) (14) and phyloseq (v1.30.0) (15) packages of the software R (https://www.r-project.org/, R 4.0.2). A total of 578 unique ASVs were retained

after filtering and rarefying. Bray Curtis dissimilarity matrix and PERMANOVA analysis were performed using the phyloseq R package. All statistical analysis on microbiome data was carried out with the software R (R 3.6.2), and statistical tests and P-values are indicated in the main text and figure legends. To identify the subset of ASVs targeted by the Bac303 and Erec482 FISH probes (Table S1), BLASTN analysis of all ASVs was performed against the respective probe sequence. This direct BLAST analysis was possible because the amplicon sequences generated with the primer pair V1-V3 include the 16S rRNA region targeted by these two FISH probes in particular (Table S1). Only ASVs aligning to the full probe sequence were retained from the BLASTN analyses. To calculate the probe coverage for the 30 top genera detected in our samples (Fig. 4D), the number of ASVs aligning to the probe sequence within each genus was divided by the total number of ASVs classified to this genus in the entire dataset.

Supporting Information Text

SRS system precision on measuring single cell metabolism activity level

In a single cell analysis of a pure culture of microbes grown under well-defined conditions, the total spread of the measurement values (σ_{tot}) is basically composed of two contributions: The heterogeneity in the metabolic activity ($\sigma_{\mathrm{metabol}}$) of the individual cells and the random measurement error of the utilized analysis technique (σ_{anal}). Based on the additivity of variances, the relationship between these quantities is given by

$$\sigma_{tot} = \sqrt{\sigma^2_{anal} + \sigma^2_{metabol}} \quad [1]$$

Here, we used SRS to probe the metabolic activity of each single cell via detection of C-D bonds formed by biotic incorporation of deuterium from heavy water into the cellular biomass, displayed as $\%\mathrm{CD}_{\mathrm{SRS}} = (\mathrm{I}_{\mathrm{CD}} - \mathrm{I}_{\mathrm{off}})/(\mathrm{I}_{\mathrm{CD}} + \mathrm{I}_{\mathrm{CH}} - 2\mathrm{I}_{\mathrm{off}})$ (see Results, Materials and Methods in the main text). The random measurement error of SRS (σ_{SRS}) is determined by several measurement parameters, such as the signal-to-noise ratio (SNR) of the utilized signals, the size of the cells (number of pixels per cell, $\mathrm{n}_{\mathrm{pix}}$), the per-pixel dwell time (t_{dw}) and the number of scans (n_{sc}) recorded for each field of view

$$\sigma_{SRS} = f(SNR, n_{pix}, t_{dw}, n_{sc}) \quad [2]$$

As a first step, we optimized the intensities of the pump and Stokes beam in combination with the per-pixel dwell time to achieve an optimum SNR without damaging the cells by the laser beams. Next, we considered the influence of the single cell measurement time (t_{m}), which consists of the product of $\mathrm{n}_{\mathrm{pix}}$, t_{dw} and n_{sc}, i.e.

$$t_m = n_{pix} t_{dw} n_{sc} \quad [3]$$

Based on the fundamental principle that the precision in estimation of the mean improves by the inverse square root of the number of measurement repetitions, the variation of the random error between two different measurements performed with t_{m1} and t_{m2} is given by

$$\sigma_{SRS}(t_{m2}) = \sqrt{\frac{t_{m1}}{t_{m2}}}\sigma_{SRS}(t_{m1}) \propto t_{m2}^{-0.5} \quad [4]$$

SRS is a non-destructive analysis technique, which means that each single cell could in principle be subjected to an unlimited number of consecutive measurements. In this hypothetical scenario ($\mathrm{t}_{\mathrm{m2}} \rightarrow \infty$), the random measurement error vanishes and the distribution of the data points exactly resembles the physiological heterogeneity within the microbial community (Eq.[1]).

In practice, the measurement time is a crucial factor in terms of throughput. In order to evaluate the essential measurement time, we analyzed two cultures of *Escherichia coli* (*E. coli*) cells grown in M9 media, one without addition of D_2O (natural isotope abundance control), and the other one after addition of heavy water (50% D_2O). For each culture, a randomly picked field of view containing 103 (natural isotope abundance control) and 58 (50% D_2O) individual cells was sequentially scanned with 10 μs per-pixel dwell time in the spectral regions of C-D, C-H and off-resonance. The two datasets were then evaluated with respect to the precision of the %CD determination for each single cell as well as the spread of the values observed across the sampled populations. Fig. S2A,B illustrates the scatter of the %CD values observed for each of the analyzed single cells (represented by the different colors). The columns on the far-left show the individual values determined in 81 scans. The consecutive columns show the values obtained from averaging over 3 up to 81 scans, corresponding to a virtual enhancement of the per-pixel dwell time from 10 μs (designated as 'Raw data') up to 810 μs (designated as '81 Avg').

Visual inspection of the charts already suggests that the spread of the single cell values continuously decreases by enhancement of the measurement time, with a more pronounced decline in the scattering of the values observed on the natural isotope abundance control. This is consistent with the hypothesis that (i) the random measurement error can be reduced by enhancement of the measurement time (Eq. [4]) and (ii) the total variance converges towards the contribution from the variation in the metabolic activity of the single cells (Eq. [1]). Fig. S2C displays the total variance, expressed as one standard deviation as a function of the average measurement time for each single cell (calculated via application of Eq. [3]). The dotted lines show the results from fitting the experimental data to a two-term power series model. For the natural abundance control, the exponent is close to -0,5 and the constant is almost negligible, which is typical for a system in which the total variance is determined by the random error of the analysis technique (c.f. Eq. [4]). The sample obtained from incubation of the cells in the isotopically enriched medium exhibits a transient behavior. If less than 3 scans are recorded, the random measurement error dominates,

which manifests itself by the overlap of the fitting curve with the curve from the natural abundance control. At 9 scans, the curve sharply levels off and approaches the value of the constant in the fitting model ($\sigma_{tot} \approx 1.0\%$CD), which refers to the extent of variation in the metabolic activity of the individual cells.

Based on these results, we decided to conduct the measurements by acquisition of 10 scans per field of view, which yields a reasonable precision in determination of the single cell values under maintenance of the exceptional throughput of the technique.

Factors determining signal intensity fluctuations in femtosecond SRS

The data plotted in Fig. 2 reveal a higher fluctuation of the SRS measurement values relative to the values obtained by spontaneous Raman, in particular for the samples incubated in media without addition of D_2O. This is due to the nature of the measurements. Briefly, in Raman spectroscopy, the intensity is derived from the integrated intensity of the C-D vibration peak after baseline subtraction. In our femtosecond SRS setup, we did not record a SRS spectrum. Instead, we recorded two intensities. One is on Raman resonance and another is off Raman resonance. The SRS signal is calculated as the on-resonance minus the off-resonance intensity. This process augments the fluctuation, particularly for the cases where the off-resonance intensity is dominant, which also becomes evident from the negative $\%CD_{SRS}$ values exhibited by cells with low D content. To address this issue, hyperspectral SRS imaging should be pursued, followed by spectral unmixing to separate the SRS signal and the non-resonant background.

SRS-FISH measurement in human gut microbiome samples

When the complex gut microbiome samples were evaluated by SRS-FISH, the TPEF signal from fluorescently labelled cells bleached much faster than in pure cultures. This might be explained by the relatively lower activity of many members of the gut microbiome, leading to a lower ribosome content and FISH signal when compared with the analyzed bacterial cultures, or by the lower cell wall permeability of particular microbiome members to oligonucleotide probes.

To overcome this limitation, we acquired the TPEF signals from microbiome samples in a dried state, without any liquid between the coverslips that carried the sample (Fig. S6A, bottom panel). Stronger and more stable fluorescence signals than in liquid conditions were obtained for both Cy3 and Cy5-labelled cells (Fig. S6B). However, the SRS signal under dried conditions is weaker due to lower laser intensity (Fig. S6, Fig. S1). We have therefore optimized our protocols to first acquire the TPEF signal from the sample in a dried form, followed by the addition of water to the sample and SRS imaging of the sample in the liquid environment (Fig. S6A, upper panel). Importantly, the percentage of the fluorescently labelled cells targeted by each of the probes in the samples, determined either by TPEF (under the dry conditions) or by confocal microscopy, was in close agreement (18.7% versus 22.9% for Bac303-Cy3, and 77.1% versus 81.3% for Erec482-Cy5; Fig. S7). In addition, we did not detect any cell-specific fluorescent signals from samples that had been hybridized with a mixture of Cy3- and Cy5-labelled negative control probes (Table S1, Fig. S7). These data suggest that the TPEF signal detected from Bac303-Cy3 and Erec482-Cy5-hybridized microbiome samples under dried conditions is accurate.

Besides, to circumvent the influence of food residues present in fecal samples on our results, the regions with overlapping signals in the Cy3 and Cy5 channels were removed from the measurement mask. Wide emission fluorescence is an indication of autofluorescence signal typically originated from food particles (16). Regions of abnormally strong intensity in the SRS image can be also attributed to the photothermal signal or transient absorption of the food residue. Therefore, intensity outliers (>mean+3SD) recorded for both C-D and C-H channels were also removed from the mask measurement results, such as the very bright spots in the negative control (H_2O+Glc) $\%CD_{SRS}$ channel in Fig. 4A.

Minimal medium for microbiome incubations

To demonstrate the applicability of the SRS-FISH approach to identify active taxa in gut microbiome samples, freshly fecal samples were collected and diluted in M9 medium containing 50% D_2O, without a carbon source added (see Materials and Methods). We chose this medium to dilute the fecal microbiome samples as it is an osmoprotective medium capable of maintaining cells alive during short incubation times (six hours incubation, in this case). Additionally, it is a defined medium extremely low in nutrients, containing only trace elements, minerals and few vitamins (see Materials and Methods), and therefore one can expect very low cellular activity and D incorporation in the absence of a carbon source or stimulant. Consistently, a negative control where D_2O was present, but no compound of interest was added, showed negligible levels of D labelling in the incubated microbiome cells (Fig. 4B, Fig. 5, Fig. S9, Fig. S11, NA condition). In contrast, when an "easy-to-metabolize" sugar like glucose was added to the M9 medium, most of the cells in the sample became active and incorporated D. For volunteer 1, under these conditions, the percentage of total microbiome cells that showed D incorporation above the threshold was higher than 95% (Figure S9). Similarly, the percentage of Bac303 and Erec482 targeted cells detected as being labelled was 90-100% (Fig. S10). This suggests that the M9 medium provides microbiome cells, including the Bac303- and Erec482-targeted taxa, with essential minerals and trace elements that enable synthesis of enzymes required for the metabolism of the substrates added. In addition to the elements provided by the M9 dilution medium, microbiome activity in incubation samples may also be sustained by residual nutrients and other elements present in the original faecal sample. As in all stable isotope probing studies, it is however possible that some organisms became D-labelled due to cross-feeding of secondary metabolites generated by primary degraders of the sugar, and not necessarily because they use the added sugar. We tried to minimize signals from cross-fed organisms in our study by using short incubation times (six hours).

We detected overall lower percentages of cells displaying D incorporation in samples originating from volunteer 3 than in samples from volunteers 1 and 2 (Fig. S9, Fig. S10). Various reasons can explain the overall lower response in volunteer 3: i) the fecal sample contained a lower fraction of viable cells at the time of collection (17); ii) the microbiome had a different composition (as shown in Fig. 4E) that may include bacteria requiring additional nutrients to become active, which are not provided by the incubation medium. Importantly, we would like to emphasize that incorporation of D does not necessarily require cell division or growth, because synthesis of macromolecules already leads to deuterium incorporation (18). Therefore, for the experiments performed in this study it is important that the selected conditions generally support microbiome metabolism leading to D incorporation (as demonstrated), but not essential that these conditions can sustain growth of all microbiome members.

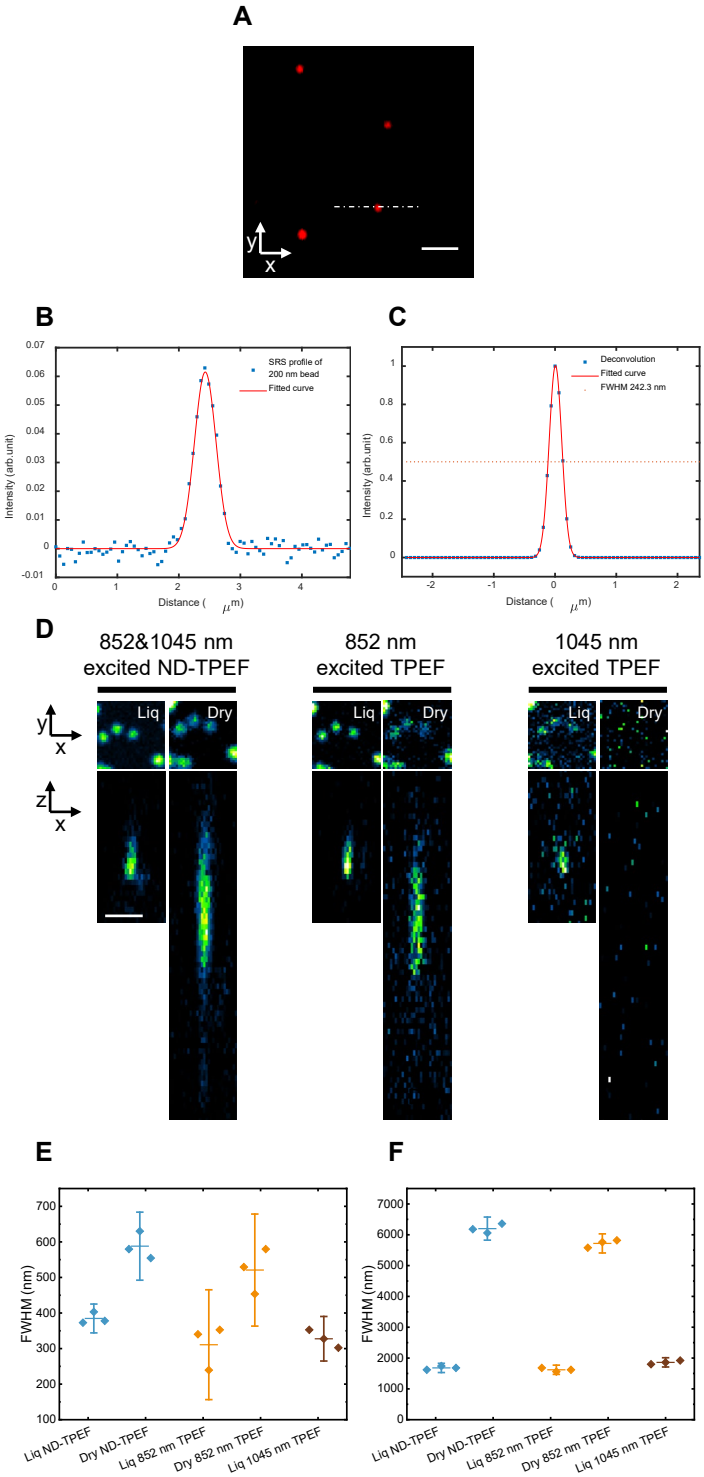

Fig. S1. Femtosecond SRS-FISH platform resolution under different sample conditions. (A) SRS imaging of 200 nm polymethyl methacrylate beads at C-H channel in lateral direction. Scale bar: 2 μm. (B) Cross section profile of the dash dot line across the bead in (A). (C) Lateral point spread function by deconvoluting the SRS image with simulated 200 nm beads. (D) TPEF imaging of 210 nm yellow green fluorescence beads with different excitations under the liquid (Liq) or dry conditions in lateral or axial directions. ND: non-degenerate. Scale bar: 2 μm. (E) lateral and (F) axial point spread function full width at half maximum (FWHM) under different excitation and sample conditions. Interval plots in (E,F) represent the mean, with the extended lines represent the value within 95% confidence interval. Diamond markers represent individual measurements.

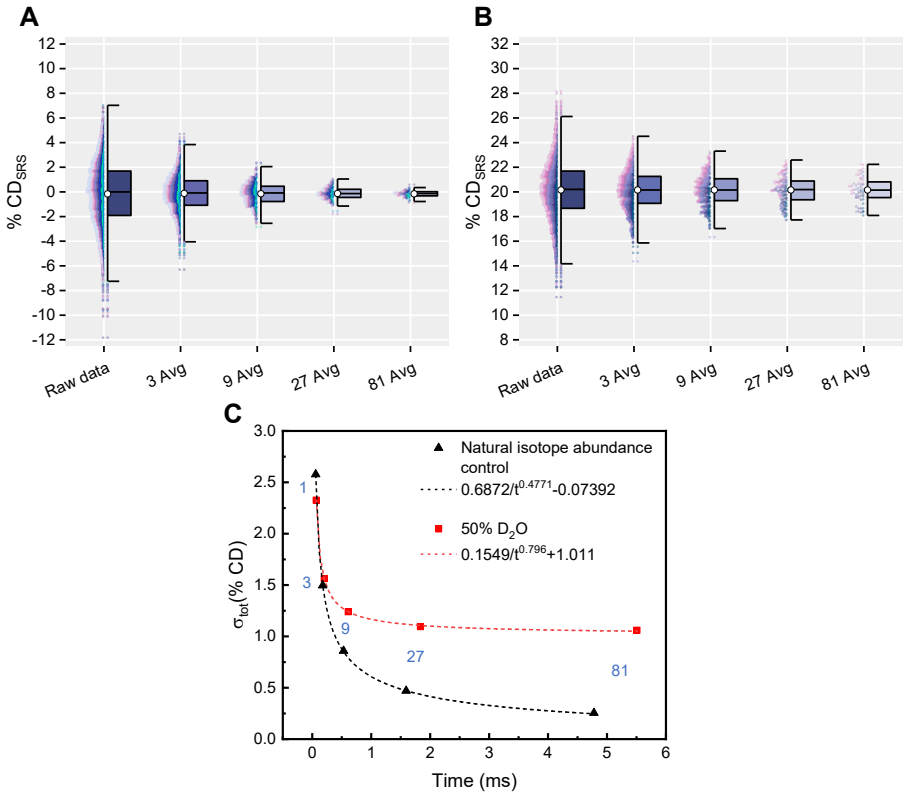

Fig. S2. Evaluation of the SRS system precision in single cell $\%\mathrm{CD}$ determination. (A,B) Single cell $\%\mathrm{CD}_{\mathrm{SRS}}$ values measured in 81 consecutive scans within a randomly chosen analysis area on samples from E. coli cell cultures grown in M9 medium without isotopic enrichment (natural isotope abundance control) (A) or with 50% $\mathrm{D_2O}$ (B). Both samples were subjected to fluorescence in situ hybridization prior to analysis. The values on the abscissa refer to the number of averaged scans. The colors of the dots, which are 103 colors for (A) and 58 colors for (B), refer to the values obtained on each of the analyzed cells. Boxes display the median, first and third quartile. Whiskers extend to the highest and lowest values that are within one and a half times the interquartile range. The white circles at the center of the boxes represent the mean of the data distribution. (C) Two-term power series model curve fitting of the standard deviations of the single cell $\%\mathrm{CD}_{\mathrm{SRS}}$ values as a function of the measurement time per cell for the two conditions shown in (A,B). The numbers in blue next to the data points refer to the corresponding number of scans.

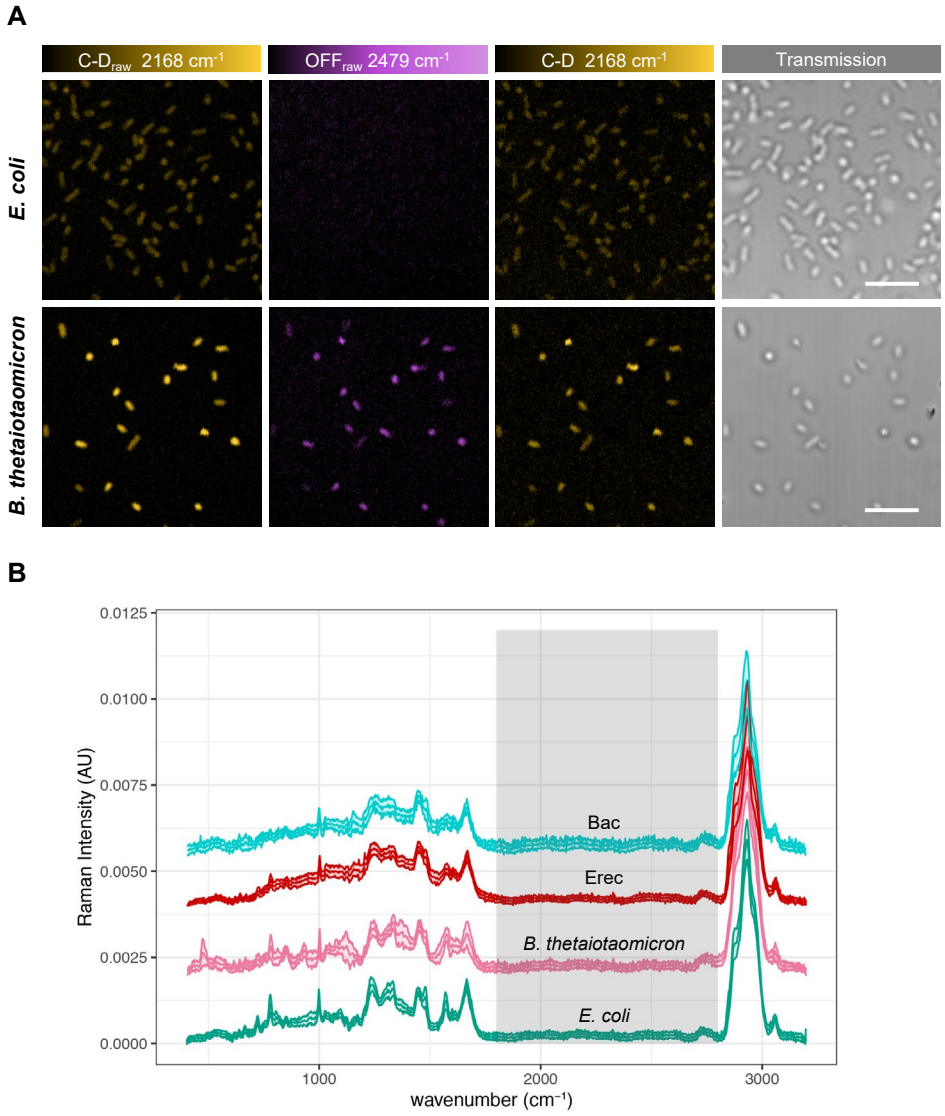

Fig. S3. (A) SRS imaging of C-D (yellow, raw and after off-resonance subtraction) and off-resonance (purple) frequencies of hybridized *E. coli* (grown in 50% D_2O-containing M9 medium) or *B. thetaiotaomicron* (grown in 50% D_2O-containing Bacteroides minimal medium) cells when imaged in liquid environment. Scale bar, 10 μm. (B) Spontaneous Raman spectra of hybridized *E. coli* (green) and *B. thetaiotaomicron* (pink) cells from pure cultures grown in H_2O-containing M9 or H_2O-containing Bacteroides minimal medium, respectively. In the same chart, spectra from cells targeted by Erec482-Cy5 (Erec, in red) and Bac303-Cy5 (Bac, in cyan) oligonucleotide probes within a gut microbiome sample incubated in H_2O-containing M9 medium are also shown. Lines depict mean values and shaded regions depict standard deviations of spectra obtained from 9-21 measured cells. The silent region between 1800 and 2800 cm^{-1} is highlighted in grey.

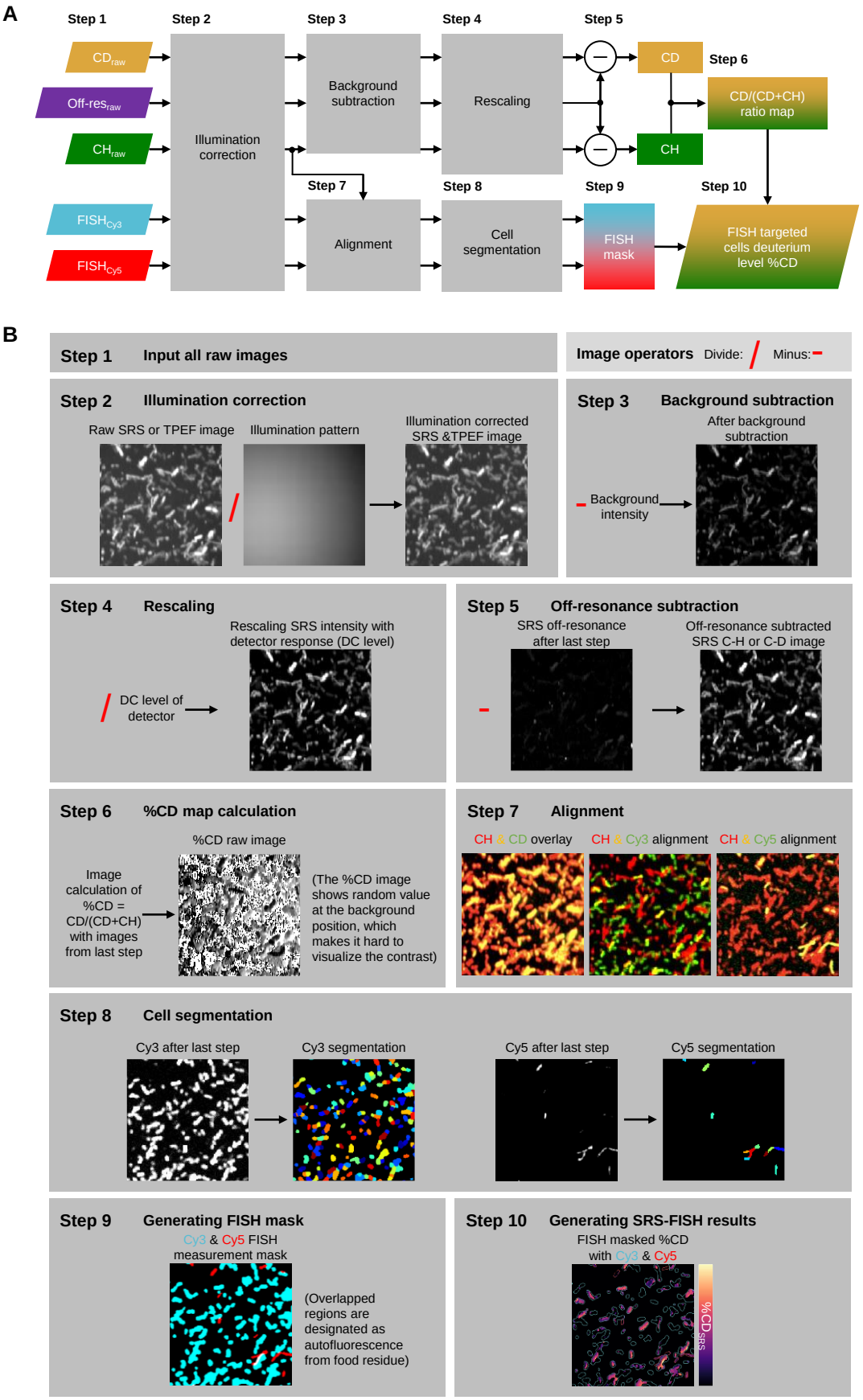

Fig. S4. Schematic representation of the strategy followed for calculation of single-cell cellular deuterium levels. (A) Image processing flowchart. (B) Operations on gut microbiome of grey boxes in (A). Detailed explanation is presented in Methods.

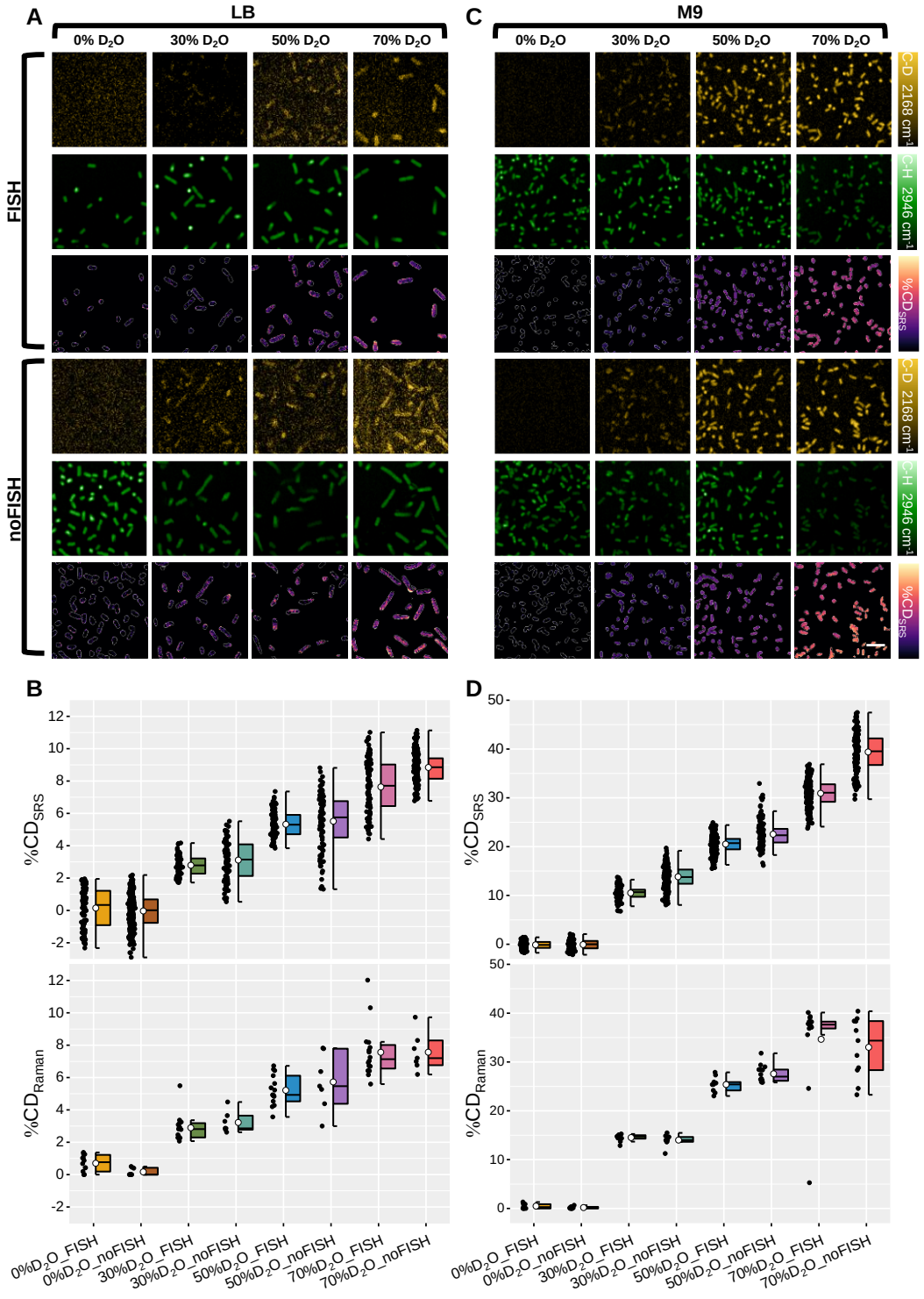

Fig. S5. SRS-FISH platform detection of $\%\mathrm{CD}$ metabolic incorporation into bacterial cells without hybridization or hybridized with oligonucleotide probes. SRS imaging of C-D (yellow), C-H (green) and $\%\mathrm{CD}$ (magma) intensities of *E. coli* cells grown in LB (A) or M9 (C) media containing increasing percentages of $\mathrm{D_2O}$. For each condition, both hybridized (FISH, top panel) and non-hybridized (no FISH, bottom panel) cells were analyzed. Cell contours are shown with gray lines. Scale bar: 10 $\mu\mathrm{m}$. Image contrast: (A) $\%\mathrm{CD_{SRS}}$: min 0, max 20%; (D) $\%\mathrm{CD_{SRS}}$: min 0, max 65%; Pixel dwell time: 100 $\mu\mathrm{s}$. For details regarding data processing please refer to Fig. S4. (B) Single cell C-D level distribution in *E. coli* cultures grown under the conditions described in A, measured with either SRS or with spontaneous Raman microspectroscopy. NS: non-significant, $\mathrm{p} > 0.05$; $*$: $10^{-5} < \mathrm{p} < 0.05$; $**$: $10^{-7} < \mathrm{p} < 10^{-5}$; $***$: $\mathrm{p} < 10^{-7}$ (two-sided Mann-Whitney U test). (D) Single cell C-D level distribution in E. coli cultures grown under the conditions described in (B), measured with either SRS or with Spontaneous Raman microspectroscopy. In (B, D) each dot represents a cell. Boxes represent median, first and third quartile. Whiskers extend to the highest and lowest values that are within one and a half times the interquartile range. The white circle in the middle of the box represents the mean value of the data.

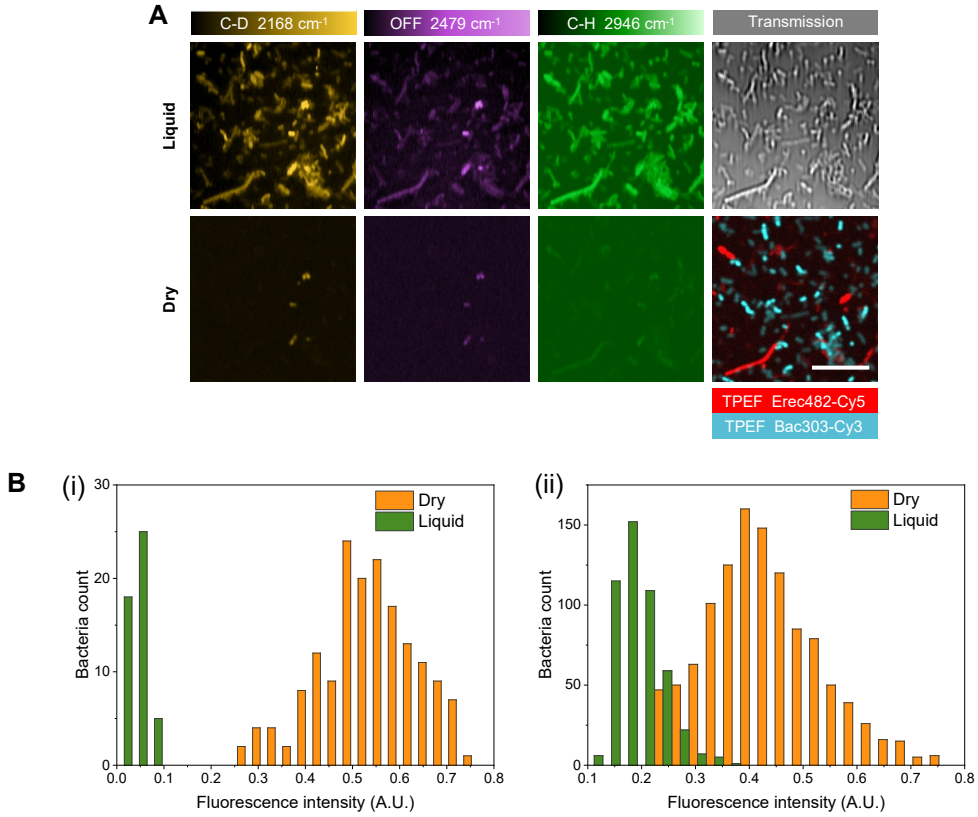

Fig. S6. (A) SRS imaging of C-D (yellow), C-H (green) and off-resonance (purple) frequencies of hybridized gut microbiome cells when imaged in liquid environment (top panel) or dry (bottom panel). TPEF signal from cells hybridized with the oligonucleotide probes Bac303-Cy3 and Erec-Cy5 is shown in cyan and red, respectively. Scale bar, 15 μm. For details regarding data processing please refer to Fig. S4. (B) Intensity distribution histogram of fluorescence signals originating from cells hybridized with Cy3- (i) and Cy5- (ii) labeled probes, when imaged in liquid or dried on a cover slide with confocal microscopy.

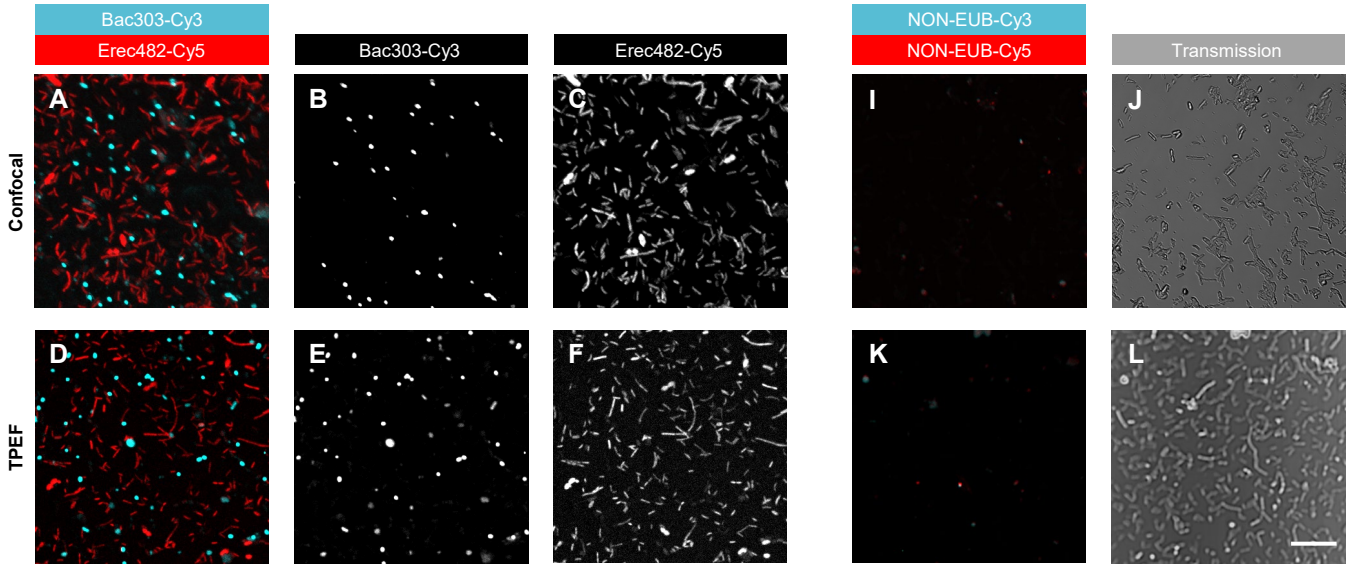

G

FOV	Bac303-Cy3: Bacteroidales	Erec482-Cy5: Clostridia
1	622 (21.9%)	2224 (78.1%)
2	538 (19.7%)	2194 (80.3%)
3	702(22.4%)	2420 (77.6%)
Total %	22.9%	77.1%

H

FOV	Bac303-Cy3: Bacteroidales	Erec482-Cy5: Clostridia
1	63 (16.4%)	322 (83.6%)
2	54 (14.7%)	314 (85.3%)
3	133 (22.8%)	450 (77.2%)
Total %	18.7%	81.3%

Fig. S7. Imaging of hybridized, fluorescently-labeled human gut microbiome samples by confocal and TPEF scanning microscopy. (A-G) Representative images of the same microbiome sample hybridized with the probes Bac303-Cy3 and Erec482-Cy5 and imaged by confocal microscopy (A-C) or by TPEF (D-F). (A,D) FISH signal under confocal (A) or TPEF (D) microscopy of Bac303-Cy3 (B,E) and Erec482-Cy5 (C,F) labeled cells. (G,H) Percentage of cells from each population (cyan-labeled or red-labeled cells divided by the number of total cyan+red cells) for 3 different fields of view (FOV), under confocal (G) or TPEF (H) microscopy. (I-L) Representative images of microbiome samples hybridized with the probes NON-EUB-Cy3 and NON-EUB-Cy5 (negative control probes employed to rule out non-specific binding of the oligonucleotide probes to cells) and imaged by confocal microscopy (I,J) or by TPEF (K,L). (I,K) Overlapped fluorescence signal under confocal (I) or TPEF (K) microscopy of Cy3 and Cy5 channels. (J,L) transmission images of (I) and (K) respectively. Scale bar: 15 μm.

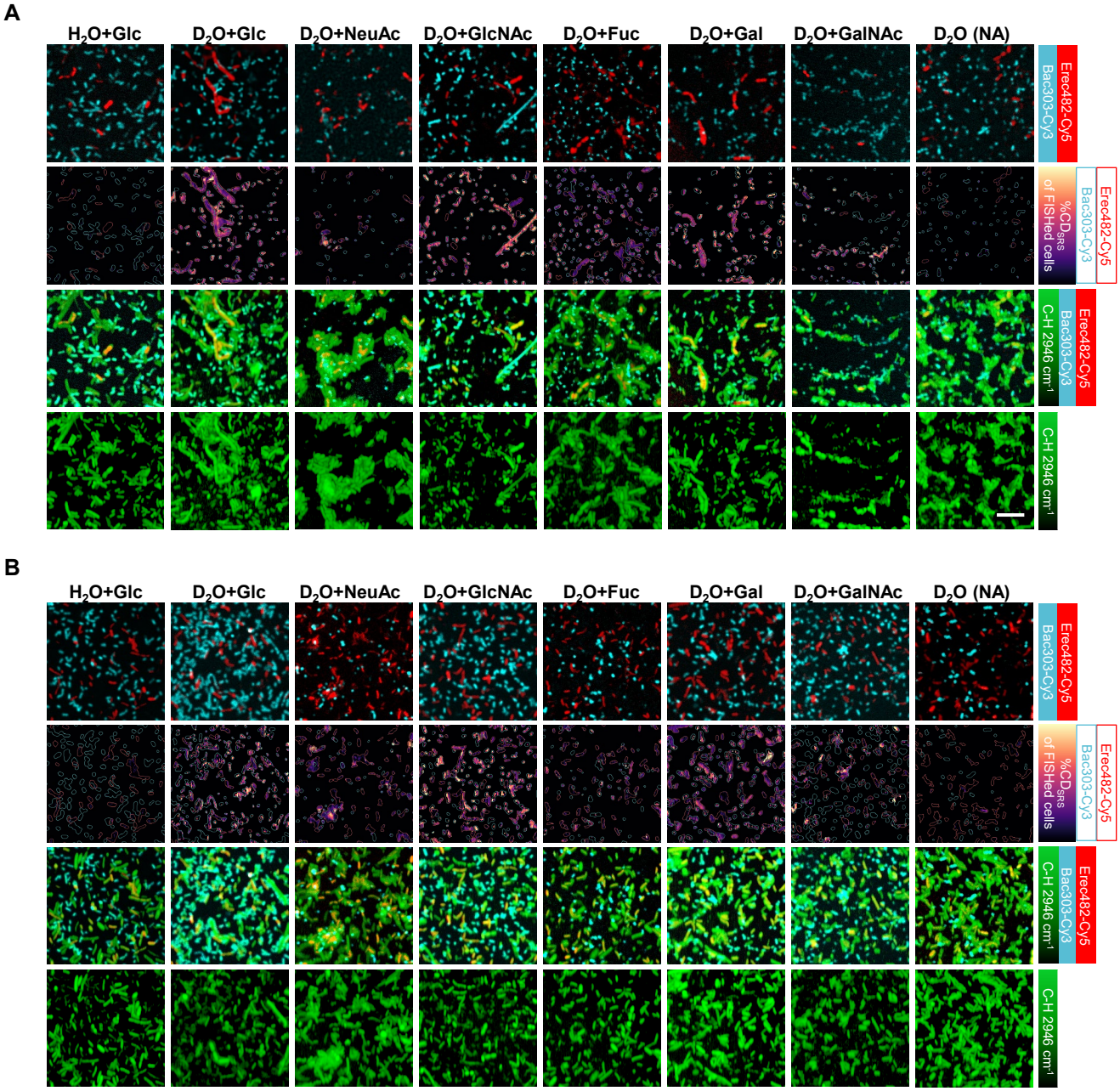

Fig. S8. Microbiome samples of volunteers 2 (A) and 3 (B) were incubated with different mucosal sugars and hybridized with the oligonucleotide probes Bac303-Cy3 and Erec482-Cy5. Representative images obtained by TPEF (top row) and SRS ($\%\mathrm{CD}_{\mathrm{SRS}}$ with FISH contours in the second row - $\%\mathrm{CD}_{\mathrm{SRS}}$ values of other microbes are not displayed to enhance clarity, C-H in log scale displaying all microbes and FISH overlay in the third row, C-H in log scale bottom row) are shown. $\%\mathrm{CD}_{\mathrm{SRS}}$ Contrast: (A) min 0, max 30%; (B) min 0, max 20%. In the second row, cells with FISH tag are shown with respective color contour lines. Negative control: $\mathrm{H_2O}$+Glucose. Positive control: $\mathrm{D_2O}$+Glucose. NA: no amendment. Scale bar, 10 $\mu\mathrm{m}$. For details regarding data processing please refer to Fig. S4.

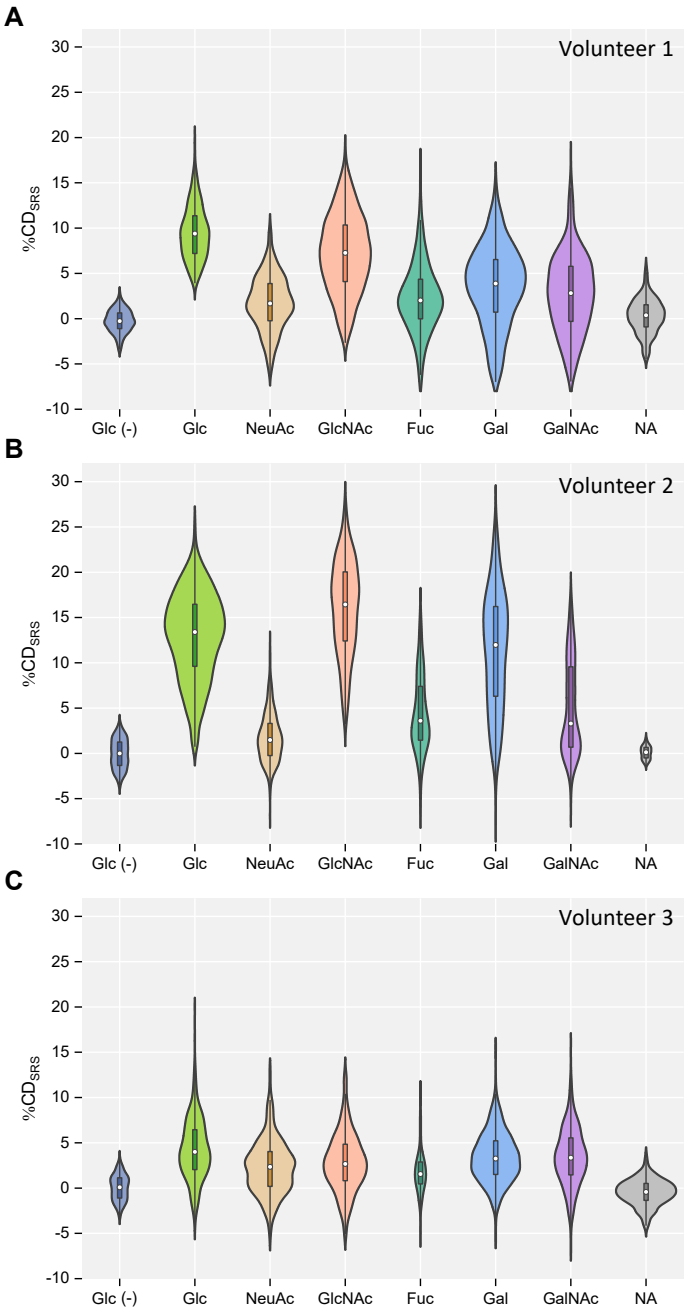

Fig. S9. Single cell C-D level distribution of all bacteria in the randomly selected field of views and amended with different mucosal sugars (and respective controls), for the same three volunteers shown in Fig. 5B. The measurement masks for the $\%\mathrm{CD}_{\mathrm{SRS}}$ levels were created with SRS C-H channel. The violin shapes represent the distribution of cells. Boxes represent first and third quartile. White dots represent median value. Whiskers extend to the highest and lowest values that are within one and a half times the interquartile range.

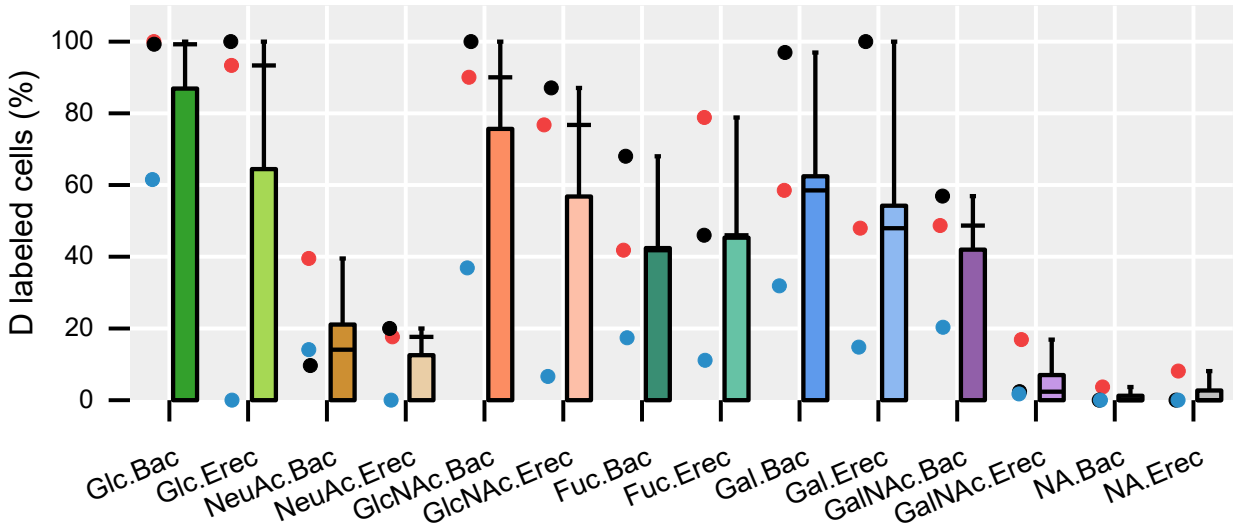

Fig. S10. Percentage of cells that show D incorporation above the threshold, determined as described in Fig. 5. The threshold corresponds to the mean $\%\mathrm{CD}_{\mathrm{SRS}}$ + 3SD of either Bac303 or Erec482 labelled cells in negative control samples. Data for the two abundant gut microbiome taxa is shown for each amended sugar (and no amendment control - NA). Bac: Bac303-Cy3 targeted cells; Erec: Erec482-Cy5 targeted cells. Each dot represents the percentage obtained for each of the three volunteers. Red dots: volunteer 1. Black dots: volunteer 2. Blue dots: volunteer 3. Bars represent mean. The intermediate lines represent the median. Whiskers extend to the values that are within one and a half times the interquartile range.

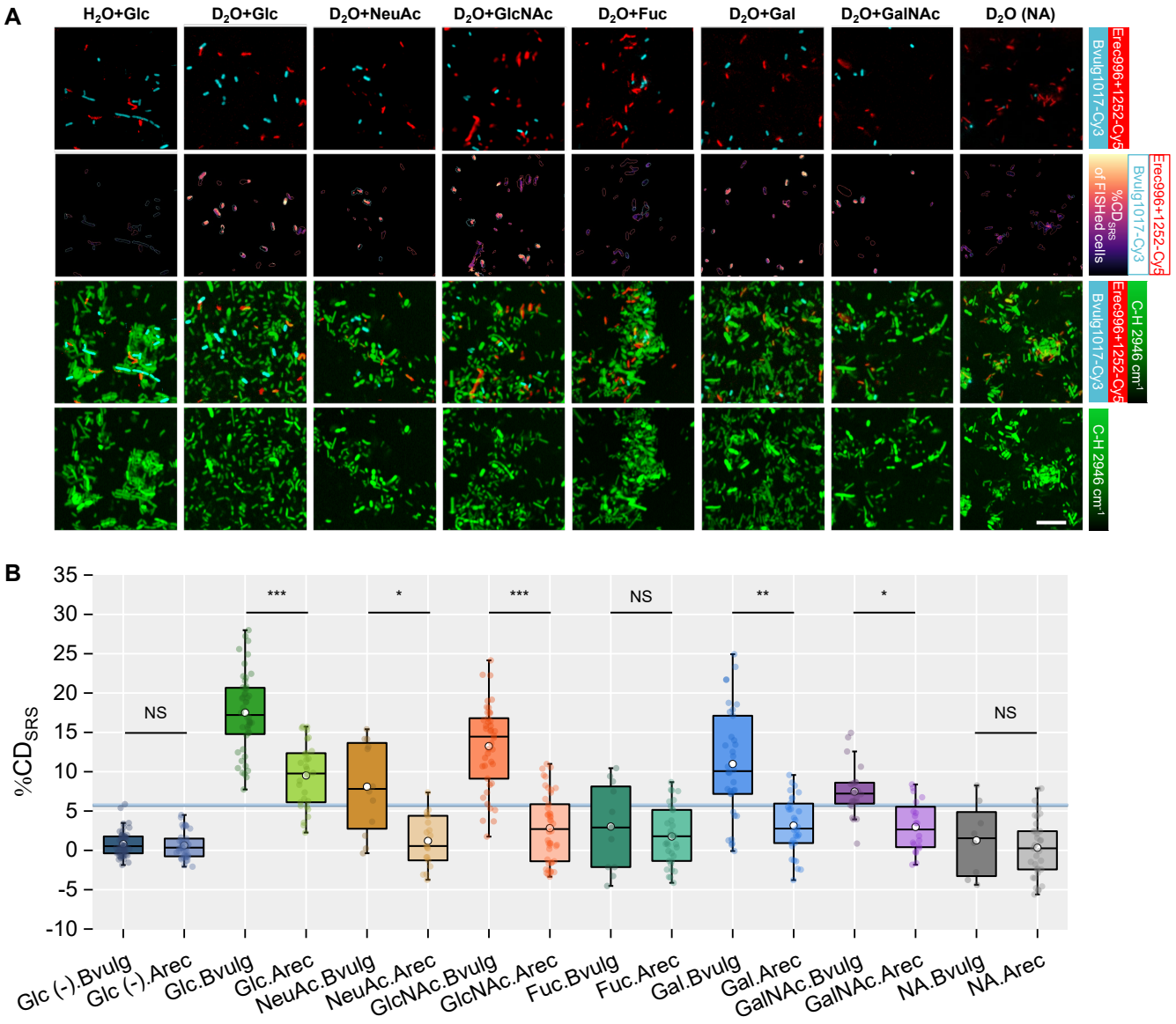

Fig. S11. SRS-FISH analysis of gut microbiome response using FISH probes with species-level resolution. (A) Microbiome samples of volunteer 2 were incubated with different mucosal sugars and hybridized with the oligonucleotide probes Bvulg1017-Cy3 and Erec996+Erec1252-Cy5 targeting two different gut microbiome species. Representative images obtained by TPEF (top row), $\%\mathrm{CD}_{\mathrm{SRS}}$ with FISH contours (second row) - $\%\mathrm{CD}_{\mathrm{SRS}}$ values of other microbes are not displayed to enhance clarity, C-H in log scale displaying all microbes and FISH overlay (third row), C-H in log scale (bottom row) are shown. In the second row, all cell contours are shown with gray lines. Negative control: $\mathrm{H_2O}$+Glucose. Positive control: $\mathrm{D_2O}$+Glucose. NA: no amendment. Scale bar, 10 $\mu\mathrm{m}$. For details regarding data processing please refer to Fig. S4. (B) Single cell C-D level distribution in the two different targeted taxa presented in (A), measured by SRS for samples from volunteer 2. Box plots represent the median, first and third quartile with the extended lines represent the minimum and maximum value within 1.5 interquartile range from the first and third quartile. The white circle in the middle of the box represents the mean value of the data. The deeper grey blue line (mean +3SD of Bvulg1017-Cy3 labelled cells in negative control) is the baseline over which Bvulg (Bvulg1017-Cy3 labelled) cells are considered labelled. The lighter grey blue line (mean +3SD of Erec996+Erec1252-Cy5 labelled cells in negative control) is the baseline over which Arec (Erec996+Erec1252-Cy5 labelled) cells are considered labelled. NS: non-significant, $\mathrm{p} > 0.05$; $*$: $10^{-5} < \mathrm{p} < 0.05$; $**$: $10^{-7} < \mathrm{p} < 10^{-5}$; $***$: $\mathrm{p} < 10^{-7}$ (two-sided Mann-Whitney U test).

Table S1. FISH probes for single cell analyses

Probe Name	Sequence (5' to 3')	Formamide (%)	Major target taxa*	Reference
Gam42a	GCCTTCCCACTTCGTTT	35	Class Gammaproteobacteria (28%)	(19)
Erec482	GCTTCTTAGTCARGTACCG	10	Order Lachnospirales (74%), Family Lachnospiraceae (75%)	(20)
Bac303	CCAATGTGGGGGACCTT	10	Order Bacteroidales (39%) Family Bacteroidaceae (86%) Family Prevotellaceae (73%) Family Barnesiellaceae (57%) Family Tannerellaceae (50%)	(21)
Bvulg1017	AGATGCCTTGCGGCTTACGGC	20	Genus *Bacteroides*(*Phocaeicola*) (41%) *Bacteroides*(*Phocaeicola*) *vulgatus*	(22)
Erec1252	CTTCACAGCTTTGCTTCCCT	20	Genus *Agathobacter* (74%) *Agathobacter rectalis*	(23)
Erec996	TTAAGTACCGGTCAGAAGGAT	20	Genus *Agathobacter* (78%) *Agathobacter rectalis*	(23)
c1Erec1252	CCTCACAGTTTGCTTCCCT	20	Competitor Erec1252	(23)
c2Erec1252	CTTCACAGCTTCGTTCCCT	20	Competitor Erec1252	(23)
NON-EUB	ACTCCTACGGGAGGCAGC	-	negative control probe complementary to EUB338	(24)

*** According to Silva database v138.1 (https://www.arb-silva.de/). The probe coverage for each taxon is shown in parenthesis. Only taxa commonly present in the human gut are presented.**

Table S2. Statistical analysis results (expressed as P-value, two-sided Mann-Whitney U test) obtained when comparing C-D levels for each sugar amendment condition with the CD levels of the negative control (Glc+H_2O). Bac: Bac303-Cy3 labeled cells. Erec: Erec482-Cy5 labeled cells. Grey background refers to p>0.05 and thus where CD levels do not significantly differ from the negative control group (Glc+H_2O).

Sugar amendment	Volunteer 1		Volunteer 2		Volunteer 3	
	Bac	Erec	Bac	Erec	Bac	Erec
Glc (+)	1.24×10^{-72}	8.20×10^{-14}	2.74×10^{-134}	4.73×10^{-31}	1.65×10^{-36}	4.66×10^{-10}
NeuAc	2.04×10^{-12}	1.09×10^{-3}	3.08×10^{-5}	8.65×10^{-3}	4.69×10^{-5}	0.890
GlcNAc	3.06×10^{-61}	1.51×10^{-11}	1.16×10^{-82}	1.06×10^{-25}	1.47×10^{-18}	1.60×10^{-3}
Fuc	1.71×10^{-13}	6.82×10^{-19}	2.28×10^{-58}	5.78×10^{-10}	1.29×10^{-3}	7.05×10^{-13}
Gal	2.11×10^{-35}	2.16×10^{-6}	4.92×10^{-90}	3.54×10^{-20}	3.64×10^{-23}	9.67×10^{-16}
GalNAc	1.01×10^{-20}	1.64×10^{-2}	1.74×10^{-70}	0.241	3.35×10^{-7}	1.75×10^{-4}
NA	0.586	0.375	0.801	0.403	0.531	0.514

References

1. J Mertz, Introduction to Optical Microscopy (2019).
2. G Wallner, R Amann, W Beisker, Optimizing fluorescent in situ hybridization with rRNA-targeted oligonucleotide probes for flow cytometric identification of microorganisms. *Cytometry* **14**, 136–143 (1993).
3. MK Bacic, CJ Smith, Laboratory Maintenance and Cultivation of Bacteroides Species. *Curr. Protoc. Microbiol.* **9**, 13C.1.1–13C.1.21 (2008).
4. S Devendran, et al., Clostridium scindens atcc 35704: integration of nutritional requirements, the complete genome sequence, and global transcriptional responses to bile acids. *Appl. environmental microbiology* **85**, e00052–19 (2019).
5. JL Maturana, JP Cárdenas, Insights on the evolutionary genomics of the blautia genus: Potential new species and genetic content among lineages. *Front. Microbiol.* **12** (2021).
6. FC Pereira, et al., Rational design of a microbial consortium of mucosal sugar utilizers reduces Clostridiodes difficile colonization. *Nat. Commun.* **11**, 5104 (2020).
7. D Berry, et al., Tracking heavy water (D2O) incorporation for identifying and sorting active microbial cells. *Proc. Natl. Acad. Sci.* **112**, E194–E203 (2015).
8. P Pjevac, et al., An economical and flexible dual barcoding, two-step pcr approach for highly multiplexed amplicon sequencing. *Front. microbiology* **12** (2021).
9. D Lane, 16s/23s rrna sequencing. *Nucleic acid techniques bacterial systematics* **.**, 115–175 (1991).
10. AE Parada, DM Needham, JA Fuhrman, Every base matters: assessing small subunit rrna primers for marine microbiomes with mock communities, time series and global field samples. *Environ. microbiology* **18**, 1403–1414 (2016).
11. CW Herbold, et al., A flexible and economical barcoding approach for highly multiplexed amplicon sequencing of diverse target genes. *Front. microbiology* **6**, 731 (2015).
12. BJ Callahan, et al., Dada2: High-resolution sample inference from illumina amplicon data. *Nat. methods* **13**, 581–583 (2016).
13. BJ Callahan, K Sankaran, JA Fukuyama, PJ McMurdie, SP Holmes, Bioconductor workflow for microbiome data analysis: from raw reads to community analyses. *F1000Research* **5** (2016).
14. J Oksanen, et al., vegan: Community ecology package. r package version 2.5-7. 2020 (2021).
15. PJ McMurdie, S Holmes, phyloseq: an r package for reproducible interactive analysis and graphics of microbiome census data. *PloS one* **8**, e61217 (2013).
16. JLM Welch, Y Hasegawa, NP McNulty, JI Gordon, GG Borisy, Spatial organization of a model 15-member human gut microbiota established in gnotobiotic mice. *Proc. Natl. Acad. Sci.* **114**, E9105–E9114 (2017).
17. CF Maurice, HJ Haiser, PJ Turnbaugh, Xenobiotics shape the physiology and gene expression of the active human gut microbiome. *Cell* **152**, 39–50 (2013).
18. D Berry, et al., Tracking heavy water (d2o) incorporation for identifying and sorting active microbial cells. *Proc. Natl. Acad. Sci.* **112**, E194–E203 (2015).
19. W Manz, R Amann, W Ludwig, M Wagner, KH Schleifer, Phylogenetic oligodeoxynucleotide probes for the major subclasses of proteobacteria: problems and solutions. *Syst. applied microbiology* **15**, 593–600 (1992).
20. AH Franks, et al., Variations of bacterial populations in human feces measured by fluorescent in situ hybridization with group-specific 16s rrna-targeted oligonucleotide probes. *Appl. environmental microbiology* **64**, 3336–3345 (1998).
21. W Manz, R Amann, W Ludwig, M Vancanneyt, KH Schleifer, Application of a suite of 16s rrna-specific oligonucleotide probes designed to investigate bacteria of the phylum cytophaga-flavobacter-bacteroides in the natural environment. *Microbiology* **142**, 1097–1106 (1996).
22. L Rigottier-Gois, V Rochet, N Garrec, A Suau, J Doré, Enumeration of bacteroides species in human faeces by fluorescent in situ hybridisation combined with flow cytometry using 16s rrna probes. *Syst. applied microbiology* **26**, 110–118 (2003).
23. BT Hanson, et al., Sulfoquinovose is a select nutrient of prominent bacteria and a source of hydrogen sulfide in the human gut. *The ISME journal* **15**, 2779–2791 (2021).
24. G Wallner, R Amann, W Beisker, Optimizing fluorescent in situ hybridization with rrna-targeted oligonucleotide probes for flow cytometric identification of microorganisms. *Cytom. The J. Int. Soc. for Anal. Cytol.* **14**, 136–143 (1993).